AIAA SciTech
13-17 January 2014, National Harbor, Maryland
55th AIAA/ASMe/ASCE/AHS/SC Structures, Structural Dynamics, and Materials Conference

AIAA 2014-0676

Analytical Correlation of a Flexible Empennage Wind Tunnel Flutter Test at High Transonic Mach Number

F. von Knoblauch[1], R. Moreno[2] and P.F. Taylor[3]
Gulfstream Aerospace Corp., Savannah, Georgia,31402,USA

J. Newsom[4]
Newsom Aerospace Consulting LLC, Poquoson, Virginia, 23662,USA

The current paper presents the correlation of a high fidelity computational aeroelastic analysis of a flexible empennage model at high transonic Mach number to wind tunnel flutter test data acquired from NASA Langley Research Center's Transonic Dynamics Tunnel (TDT).

I. INTRODUCTION

CURRENTLY, industry mainly relies on the conventional Doublet Lattice Method (DLM) to model the unsteady aerodynamics of lifting surfaces and bodies, due to its reduced cost and its relatively good representation of the lags between the surface motion and the aerodynamic forces. As the DLM is based on potential theory, it is not capable of capturing complex three dimensional, compressible or viscous effects. A variety of methods to correct the linear theory exist. It is standard industry practice to correct the absolute value of the aerodynamic forces based on steady aerodynamics, often gained by computational fluid dynamics calculations and rely on the DLM phase lags. This combination is possibly the cheapest unsteady aerodynamic method in terms of computing requirements. This makes the running of thousands of flight cases possible for both flutter and dynamic flight loads. One drawback to this method is the lack of theoretical basis for considering that the unsteady effects are independent of viscosity and compressibility. These effects are traditionally considered as having a major influence on the flutter characteristics of lifting surfaces, even more so when the flutter mechanism involves control surface rotation or deformation, as the shock movement drastically changes the control surface aerodynamic characteristics. Such shock motion is deemed to be highly influenced by the high reduced frequencies of the motion. The complexity of the unsteady aerodynamic phenomena which show up in the transonic speed range make extensive wind tunnel testing highly desirable both to design optimum structures and to reduce the certification risks, as well as to meet the FAA's mandate for analyses backed up by testing [1].

One way to overcome the aerodynamic uncertainty is through the use of Computational Fluid Dynamics (CFD) codes coupled with a flexible structure finite element analysis (FEA). However the current high computational cost involving a fluid-structure interaction simulation using CFD makes it not feasible to use this method for industrial flutter calculations. For this reason it is often used only in research or cases with conditions including flow separation or buffeting, which would involve many thousands of computations, where the linearized aerodynamic method is not applicable. But in any case, the lack of maturity and validation of fluid-structure interaction codes prevents the trust of the outcome.

In this paper a high fidelity computational aeroelasticity method is compared to the acquired test data from a flexible empennage model. Gulfstream conceived and executed a wind tunnel test campaign at NASA Langley Research Center's specialized aeroelastic testing wind tunnel known as the Transonic Dynamics Tunnel (TDT) [2]. The analysis of this acquired data will not only allow Gulfstream's Loads and Dynamics department to reduce the uncertainty in unsteady aerodynamic forces at transonic speeds and validate the current state of the art methodology

---

[1] Technical Specialist, Loads and Dynamics.
[2] Technical Specialist, Loads and Dynamics. AIAA Senior Member
[3] Principal Engineer, Loads and Dynamics. AIAA Associate Fellow
[4] Consulting Engineer. AIAA Associate Fellow.

but will also allow the validation of the fluid-structure interaction method used in this paper. Test points showing both stable and unstable behavior are selected from the wind tunnel database and a coupled fluid-structure aeroelastic analysis is performed using NASA's unsteady Navier-Stokes solver FUN3D [3] [4]. A linear structure is assumed for this application and the structural dynamics equations in generalized coordinates are solved internally in FUN3D. The structural inputs to the aeroelastic solver are computed with MSC NASTRAN [5].

II. METHOD OF ANALYSIS

A coupled fluid-structure aeroelastic analysis is computationally a very demanding calculation and for this reason it is mainly used in research and for investigation of limited conditions due to the length of time required and availability of computational resources. NASA's unsteady Navier-Stokes solver FUN3D has been used, since it includes a fairly complete aeroelastic module. The structural inputs to the aeroelastic solver consist of the eigenvectors, eigenvalues and generalized masses of a ground vibration test (GVT) correlated finite element model (FEM). The structural modes are mapped onto the aerodynamic mesh using an interpolation scheme, based on Wendland's radial basis functions as implemented in MSC NASTRAN.

After each time step the aerodynamic loading from the unsteady Reynolds-Averaged Navier-Stokes (uRANS) solution is transformed into generalized forces and the structural dynamics equations are solved. The corresponding generalized displacements are multiplied with the appropriate eigenmodes. The deformed shape is the summation of the weighted eigenmodes. The actual deformation of the aerodynamic mesh, invoked within FUN3D, is treated as a linear elasticity problem using the generalized minimum residual (GMRES) method [6]. The new mesh based on the deformed shape is the starting point of the next time step of the uRANS simulation. The process repeats until the specified number of time steps is reached.

To avoid large deformations caused by transient solutions leading to potential termination of the analysis due to negative mesh volumes a three-step process has been followed, as suggested in Reference [7]. Firstly, an initial aerodynamic loading is determined running a steady state, rigid solution. In the second step the CFD analysis continues in a time accurate mode using a high value for structural damping. After the aeroelastic system comes to static equilibrium, the structural damping is set back to 0.0 and an initial perturbation in the form of a generalized velocity for each mode is applied. The time step size is determined by resolving the modal frequency for the relevant mode into 100 time steps per cycle. The flow chart in Figure 1 explains the dynamic aeroelastic analysis, which is step 3 of the described process.

The outputs of the analysis are the time varying generalized co-ordinates, generalized velocities and generalized forces. In the case of a stable condition the amplitude of the generalized co-ordinates for all modes must decay. To determine the dominant frequency the time traces are converted into the frequency domain using the fast fourier transform algorithm (FFT) in Matlab [8]. Also for selected cases the damping ratio is calculated from the generalized co-ordinate time history using the logarithmic decrement method [9]. A positive damping ratio indicates a stable solution and for an unstable solution the damping ratio is less than zero.

Table 1 presents a summary of the execution times for the mesh used in this paper. Depending on the convergence time needed for the mesh movement and the time step size to resolve the relevant frequency these values may vary slightly.

Table 1. Typical Execution Times for the Analysis

Description	cpu time	Processors (Intel Xeon @ 2.5 GHz)
Step 1: Rigid Run	1 hour	120
Step 2: Static Run	10 hours	240
Step 3: Dynamic Run	25 hours	240

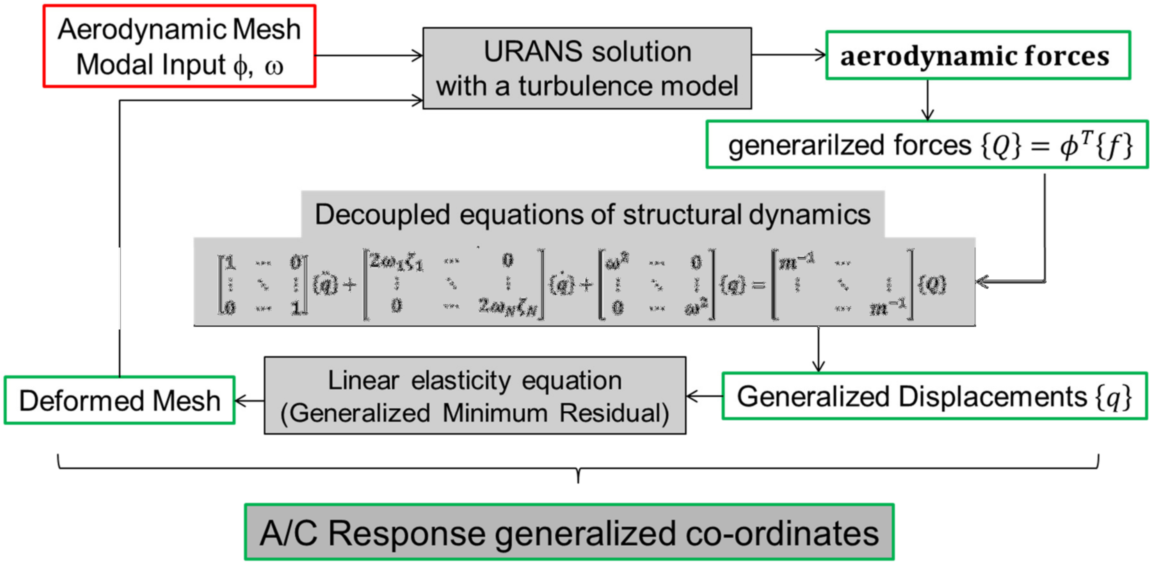

Figure 1. Aeroelastic Analysis Process

III. MODELS

The empennage configuration has been chosen as it generally provides the most critical flutter margins and typically involves coupled main surface and control surface rotation flutter mechanism. The configuration is generic and does not represent an actual Gulfstream configuration. The goal of the model design was to exhibit the same flutter mechanism as the full scale generic configuration and to have flutter to occur well within the TDT operating envelope at a moderate dynamic pressure. The model scale is approximately based on the empennage size of the various Gulfstream large cabin series of aircraft and is assumed to be 25%. The design and construction of the model was done by NextGen Aeronautics, Torrance, California and a more comprehensive description can be found in [10].

A. Wind Tunnel Model and Test Data

Figure 2 shows the complete model installed in the NASA Langley Transonic Dynamics Tunnel (TDT). The wind tunnel model structure consists of three main components: the horizontal stabilizer (HS) and elevators, the vertical stabilizer (VS) and a rigid base structure. The base was finished with a fiberglass aerodynamic fairing and attaches the model to the tunnel floor. The outer mold line shape was achieved by covering the aluminum plate structure with machined high density foam.

The primary measure of response was from the array of 25 accelerometers placed throughout the model. Accelerometers were placed in a chordwise and spanwise distribution on the starboard horizontal stabilizer at 10 and 65% chord and 25, 50, 75 and 90% of the span. On the port side, only the 50% and tip locations were duplicated to characterize whether dynamic response was symmetric or anti-symmetric. Accelerometers were placed on the same spanwise location on both elevators at approximately 50% of the elevator chord. Figure 3 shows the HS accelerometer locations.

The test was conducted using heavy gas (R-134a) as the test medium in the TDT. The tunnel is equipped with four by-pass valves. In the event of model instability the activation of the valves is causing a rapid reduction in the test section Mach number and dynamic pressure that serves to potentially stabilize the model. However for a mechanism in the 50 Hz range the manual activation of the valves might not be quick enough. To mitigate the risk of model damage a set of aerodynamic exciter vanes were incorporated at each HS tip, as shown in Figure 4. These vanes allowed excitation of the model over a large frequency range. More details concerning the wind-tunnel model and test are described in [10]. All test points are plotted in Figure 5, with the hard flutter points identified by large symbols.

Figure 2. Model Installed in TDT Test Section

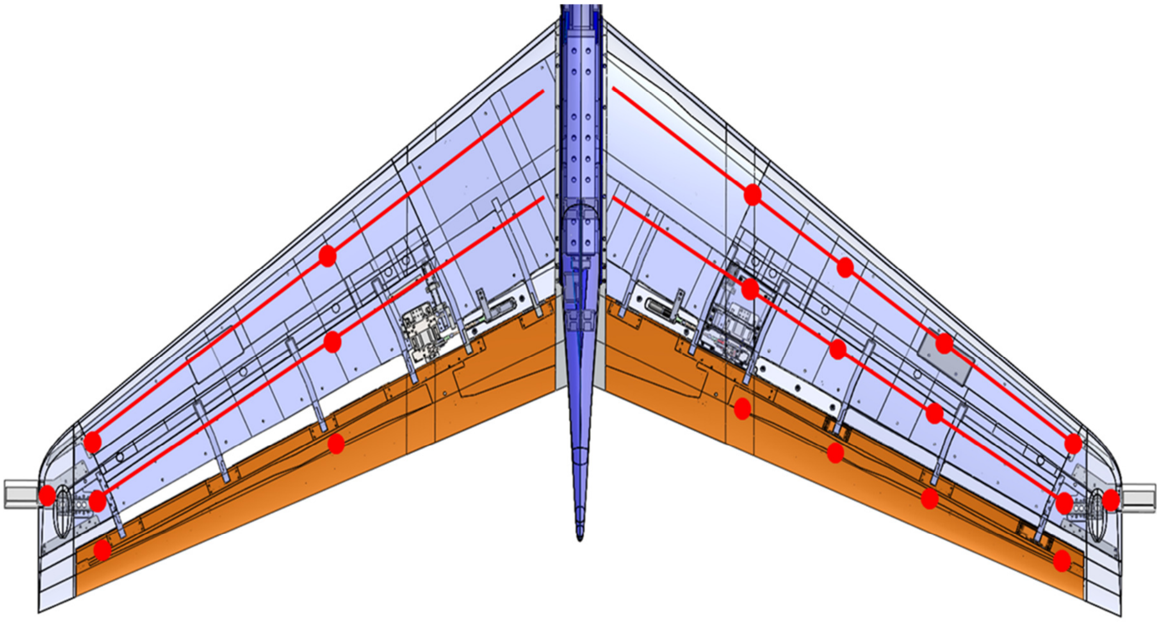

Figure 3. Accelerometer Locations on Horizontal Stabilizer

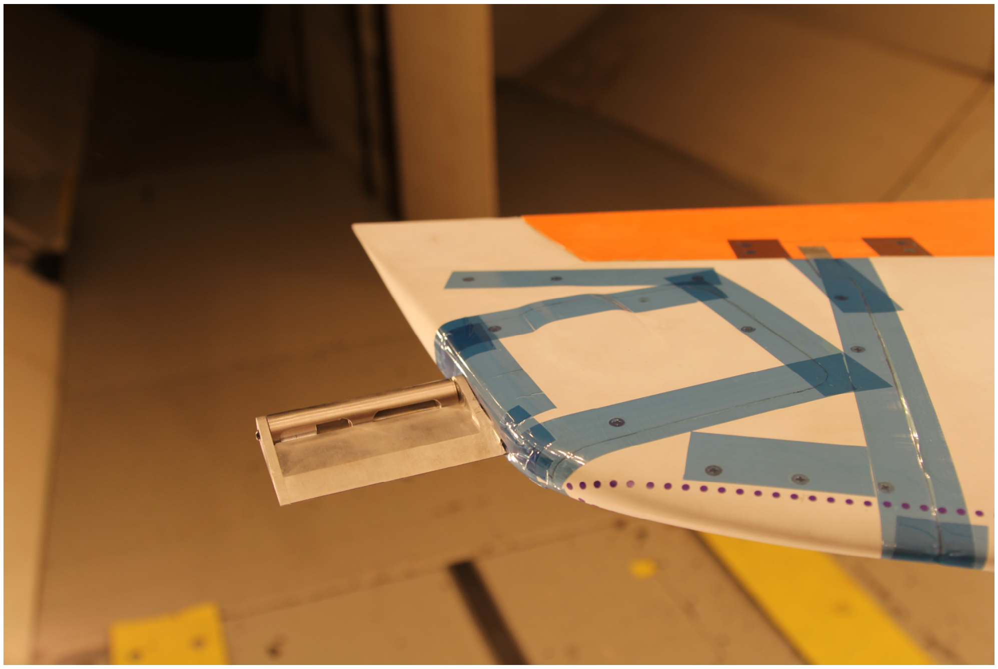

Figure 4. Flutter Excitation Vane

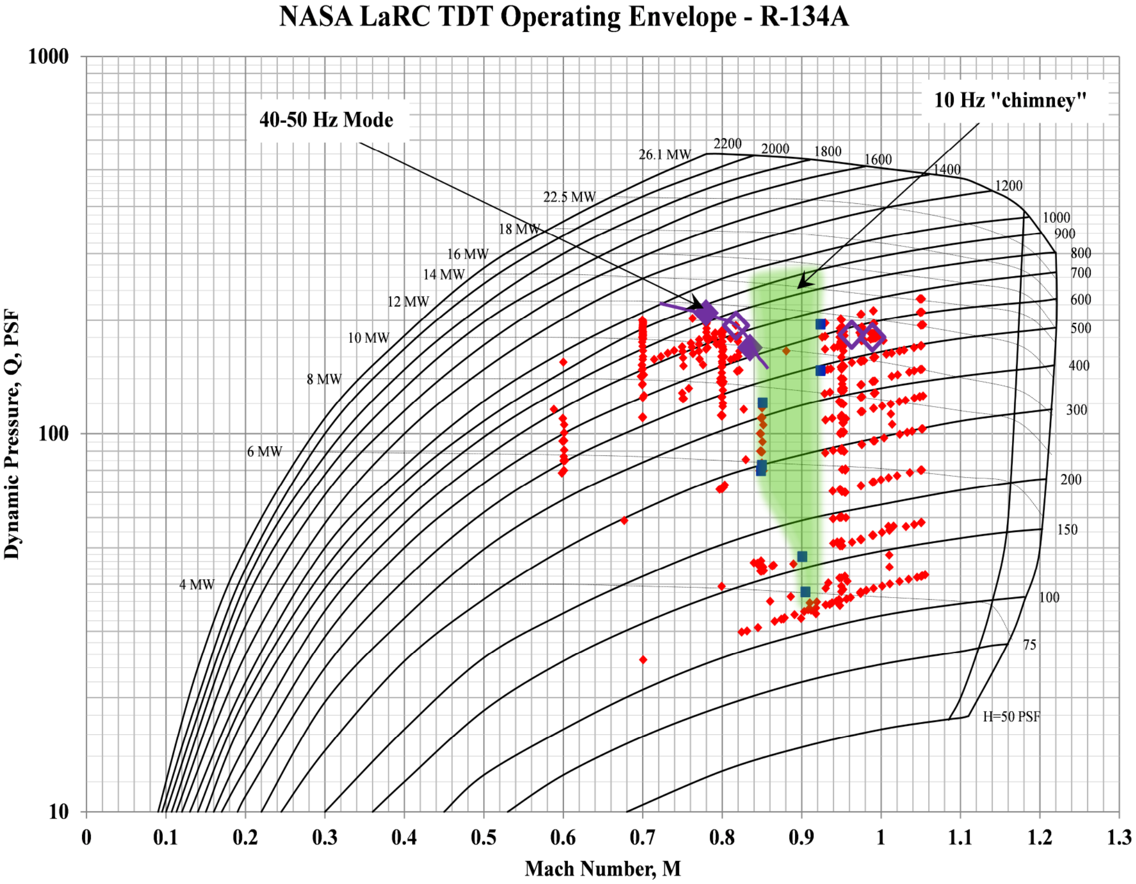

Figure 5. TDT Envelope Including Test Points

B. Aerodynamic Model

The RANS equations were solved using the NASA FUN3D flow solver. Turbulence closure was obtained using the Spalart-Allmaras [11] one-equation model. Roe flux difference splitting without a reconstruction limiter has been selected to reconstruct the flux. The flow parameters are set to replicate the wind tunnel flow characteristics. The unstructured tetrahedral grids used were generated with the mesh generator Pointwise [12]. The mesh domain is approximately 100 root chords width by 100 root chords long by 50 chords height, as recommended in the drag prediction workshop [13]. A viscous boundary layer has been selected for the entire model including the fairing. The tunnel floor has been defined as an inviscid wall. Farfield-Rieman boundary conditions have been imposed in the box. The boundary layer grid was converted into prism leading to a mesh size of 15.7 Million cells. The aerodynamic surface mesh for the complete wind tunnel model and a more detailed view on the horizontal tail is shown in Figure 6. Selected points have been analyzed for a fine mesh double the size of the mesh in Figure 6, but the outcome of the stability analysis did not differ.

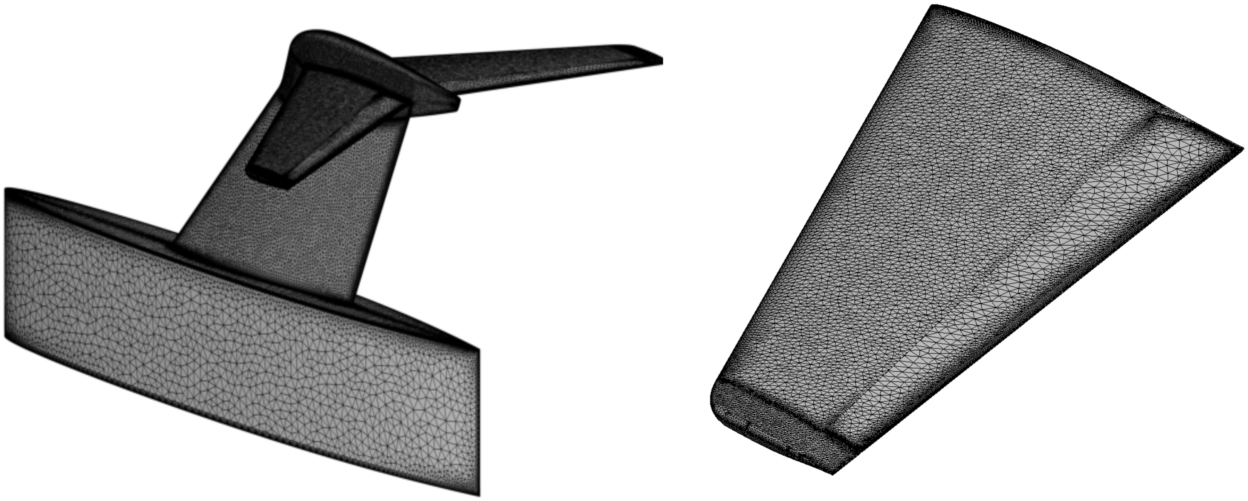

Figure 6. Aerodynamic Surface Mesh

C. Structural Model

Several component vibration tests were conducted to allow a correlation of the major components modal characteristics individually. Finally a ground vibration test (GVT) of the assembled model in the Model Preparation Area (MPA) of the TDT prior to installation in the test section allowed a tuning of the complete FEM (primary connections between component) used in the analyses.

A modal analysis of the GVT correlated model is performed as a pre-processing step using MSC NASTRAN (SOL 103). The solid element finite element model (FEM) of the structure containing 2 million nodes and 650.000 tetrahedral elements is shown in Figure 7. The model includes TDT test section floor structure and substructure considered potentially important in the dynamic analyses of the model and floor connection. In Table 2 selected relevant modes gained from the structural analysis are compared to same modes extracted from a ground vibration test (GVT). Due to complexity of the elevator actuator mechanism it was not possible to achieve the same frequency for both elevator rotations, as it was very sensitive to tolerances stack-up. In the aeroelastic analysis the first 22 modes, capturing a frequency range up to 100 Hz were used.

Table 2. Finite Element Model Correlation to Ground Vibration Test

Description	Test Frequency, Hz	FEM Frequency, Hz	Modal Assurance Criteria (MAC)
HS Symmetric Bending	8.3	8.3	0.98
Starboard Elevator Rotation	36.1	35.9	0.89
Port Elevator Rotation	39.2	39.2	0.84
HS Torsion	59.0	59.3	0.82

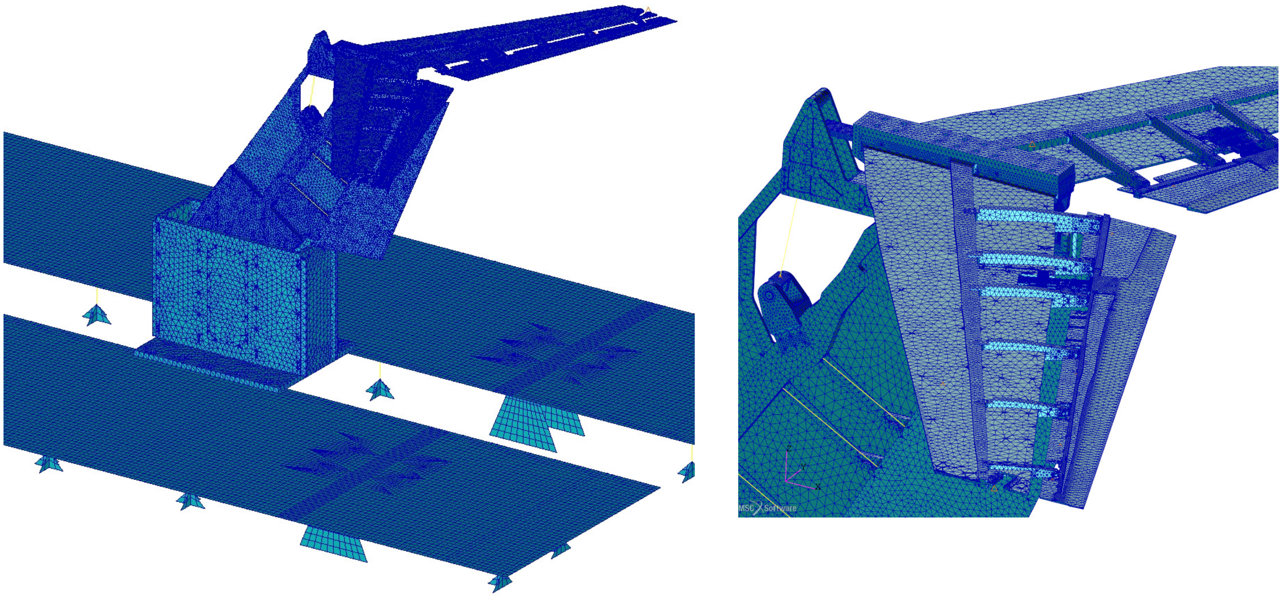

Figure 7. Finite Element Analysis Model

D. Mapping Mode Shapes

The mode shapes were mapped from the structural mesh to the aerodynamic mesh using an interpolation scheme, based on Wendland's radial basis functions, as implemented in MSC NASTRAN SPLINE4 card. Initially the mode shapes from the structural analysis were mapped onto the CFD mesh including the VT. However in this process FUN3D failed during the unsteady flow solution due to negative volume at the VS-fairing interface. The failure could be caused by the discontinuity of the mode shape due to differences between the structural and the aerodynamic model, as also suggested in Reference [7]. Since the relevant flutter mechanism had little VS involvement, the moving components were restricted to the HS and the bullet fairing. This approach proved to result in a successful execution of the aeroelastic analyses.

Figure 8 and Figure 9 show the symmetric HS bending mode and the port elevator rotation mode, respectively mapped from the structural mesh on the left to the aerodynamic mesh on the right. The shapes on the two different grids compare well.

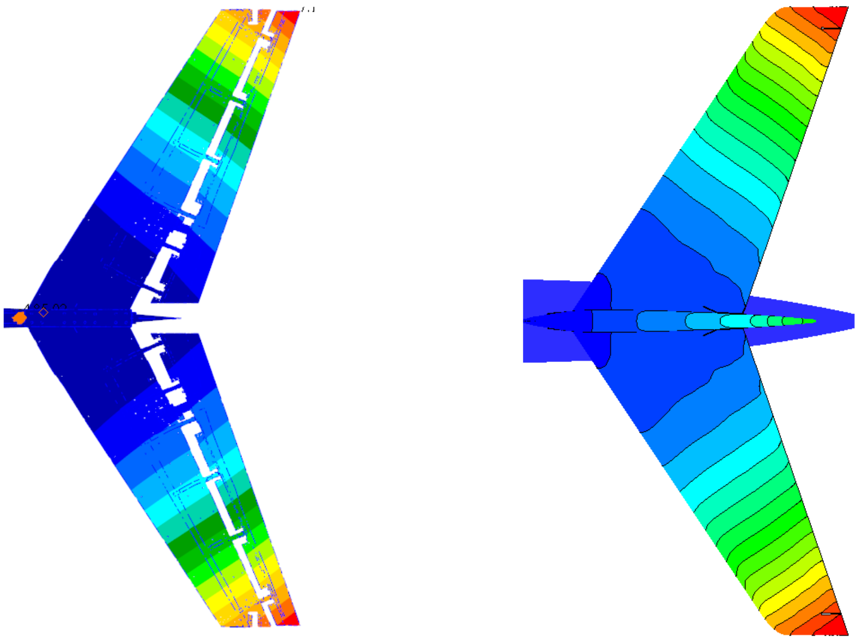

(a) Symmetric Bending Mode on FEM (b) Symmetric Bending on Aerodynamic Mesh

Figure 8. Horizontal Stabilizer Symmetrical Bending Mode mapped from FEM to CFD Mesh

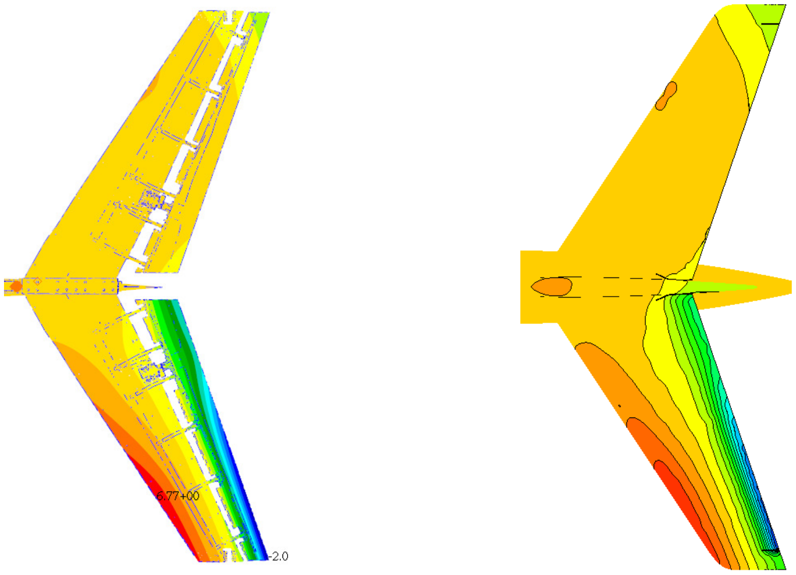

(a) Elevator Mode on FEM (b) Elevator Mode on Aerodynamic Mesh

Figure 9. Port Elevator Rotational Mode mapped from FEM to CFD Mesh

IV. RESULTS

The first mechanism encountered during testing was an unexpected 10 Hz instability around a Mach Number of M=0.9. As measured in the wind tunnel the instability was not present below M=0.85 nor above M=0.92 (actual numbers vary slightly with dynamic pressure). Post-test CFD analyses indicate this phenomenon was a single degree of freedom instability of the first symmetric horizontal tail bending, which may be caused by a shock wave emanating from the bottom fairing, impinging on the horizontal stabilizer. When the flow Mach number is between 0.85 – 0.92 the shock moves to the critical location on the underside of the HT and triggers the 10 Hz mode.

Figure 5 shows a schematic of the boundary superimposed on the TDT operating envelope in the heavy gas test medium. The 10 Hz instability split the test envelope into two parts, the high speed regime above M=0.92 and the low speed up to M=0.85. Traversing across the “chimney” shown as a green shaded area in Figure 5, was not possible due to the instability. A way which was devised during testing, to get to the high speed section was to start at very low dynamic pressure (typically less or equal to 30 psf) and increase the fan speed rapidly to get above M=0.92. The focus in sub-section A-C is the 10 Hz instability. In sub-section A the analytical results are compared to the test data for two Mach Numbers at this low dynamic pressure. In the following sub-sections B and C the analytical results for a dynamic pressure of 100 and 150 psf, respectively, are compared for a variety of Mach numbers to the wind tunnel data.

The second mechanism measured was the desired 40-50 Hz coupled horizontal stabilizer torsion and elevator rotation. Two hard flutter points have been measured. The first one for M=0.833 at a dynamic pressure of 168 psf and the second for M=0.78 at a dynamic pressure of 208 psf. In sub-section D-E the analytical results for these Mach Numbers varying the dynamic pressure are compared to the wind tunnel data. Due to safety and large model responses sometimes the test was potentially stopped too early. During post-processing the test data some points left the question open whether the case was an unstable oscillatory condition. The structural damping used for the analytical cases was set to zero.

A. Mach Number Variation for q=30 psf

Figure 10 shows time traces from the wind tunnel test for M=0.85 on the left and M=0.9 on the right. The amplitudes of the accelerometer time histories for the port tail tip at 65 % chord (APSTPZ65) on the top of the figure are small and damped out for M=0.85, the model is stable for this condition. Since the HS bending mode was dominant the tail tip acceleration with the maximum response has been selected, however the other accelerometer locations show the same behavior. Test point 477 at M=0.9 shows a very low damped to neutral condition. Power spectral densities (PSD) of the time histories illustrated on the bottom of the Figure 10 confirm the 10 Hz mode being dominant.

In Figure 11 the analytical results for M=0.85 and M=0.9 are presented. On the top, the generalized displacement for the relevant mode is shown, in this case the horizontal symmetric bending, and on the bottom the corresponding PSD for the time history. Both the wind tunnel and the CFD analysis show a stable behavior for M=0.85. The dominant frequency is around 8.8 Hz and matches the frequency determined from the test data well. On the right hand side of Figure 11 the Mach number is matched to test point 477 and as seen in the test, the model shows a neutral behavior. The amplitude of the generalized co-ordinates is neither decaying nor increasing. The dominant frequency increased insignificantly. For higher Mach numbers the analytical model also returned to a stable condition.

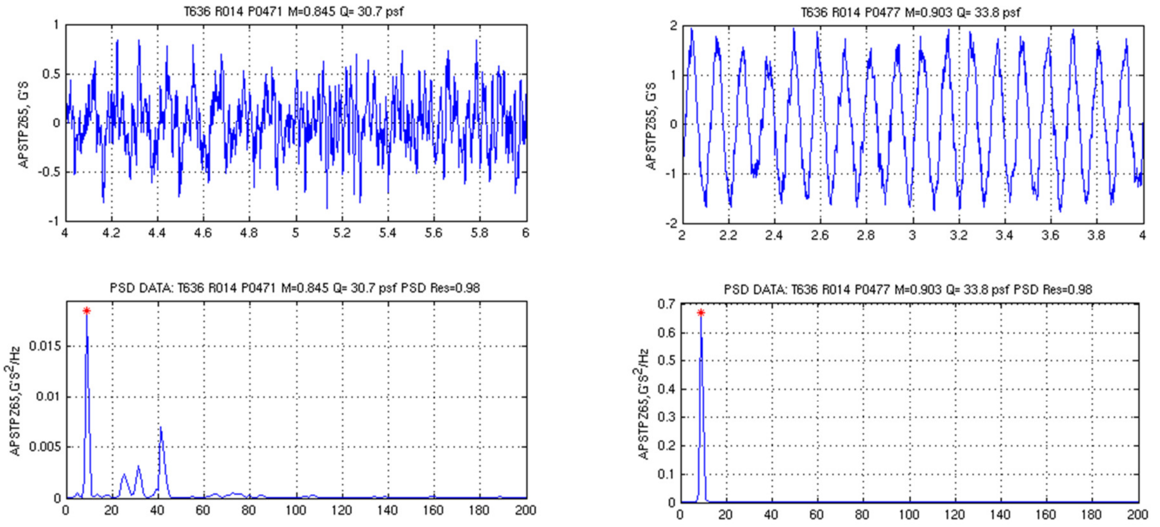

(a) Test Point 471, M=0.85, q=30 psf, f=8.79 Hz

(b) Test Point 477, M=0.9, q=30 psf, f=8.79 Hz

Figure 10. Test Results for q=30 psf

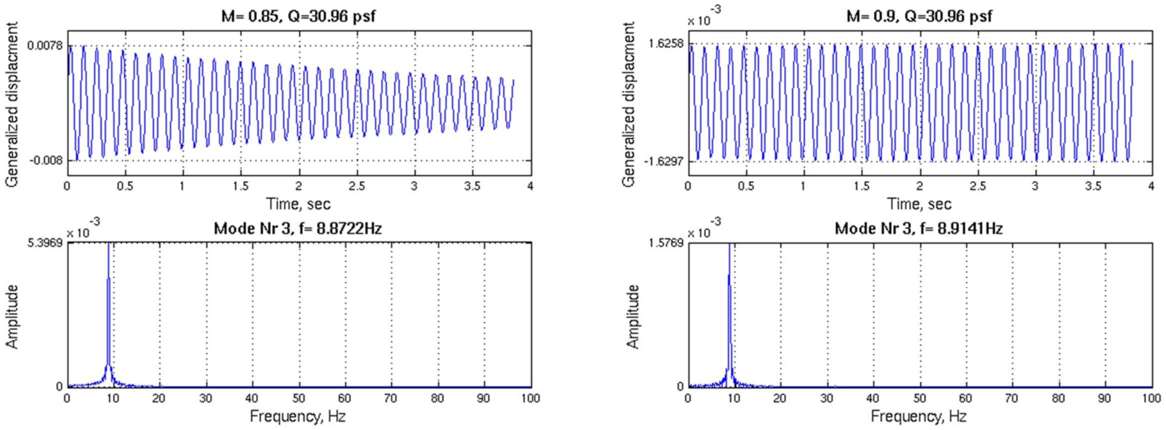

(a) M=0.85, q=30 psf

(b) M=0.9, q=30 psf

Figure 11. Analysis Results for the HS Symmetric Bending Mode, q=30 psf

B. Mach Number Variation for q=100 psf

In this section the analysis was performed for a variation of Mach numbers starting at M=0.85 up to M=0.95 keeping the dynamic pressure constant at q=100 psf. The aim of this section was to reproduce the 10 Hz instability for M=0.9 seen during testing but also to explore the instability boundaries for a dynamic pressure of q=100 psf. Determining the 10 Hz instability form the test proved to be more challenging due to the existence of buffet in the data, high amplitudes and the risk to the model.

In Figure 12 the generalized co-ordinates for the symmetric horizontal tail bending mode are plotted for the various Mach numbers. As experienced in the wind tunnel the top right graph in Figure 12 confirms a 10.2 Hz instability for M=0.9. By reducing the Mach number to M=0.85 the amplitude of the model response decays and the model shows a stable behavior. By increasing the Mach number up to M=0.93 the 10 Hz mode seems to be damped out too, however a high frequency low amplitude buffeting, as illustrated in Figure 13 is present in the HS torsional mode. The damping trend in Figure 17 was extracted from the analysis using the logarithmic decrement method. A negative damping ratio indicates an unstable condition. The analyses suggest a 10 Hz instability region between M=0.875- 0.91. Like the test, the CFD analysis also did not show the 10 Hz instability for M= 0.85.

Figure 14 shows the time trace for the port tail tip accelerometer at 65 % chord (APSTPZ65). After a second, the tip exciter (TESPSPD) is activated for 5 seconds. After switching the exciter off, the acceleration decayed and the model returned to a stable condition. For the higher Mach numbers there was a lot of buffeting in the test data and in the analysis results. The time traces in Figure 15 and Figure 16 show a beating phenomenon of the HS bending mode for M=0.93 and M=0.95 respectively, suggesting the cases were only marginally stable. The 10 Hz instability boundary for q=100 psf between test and analysis matches well.

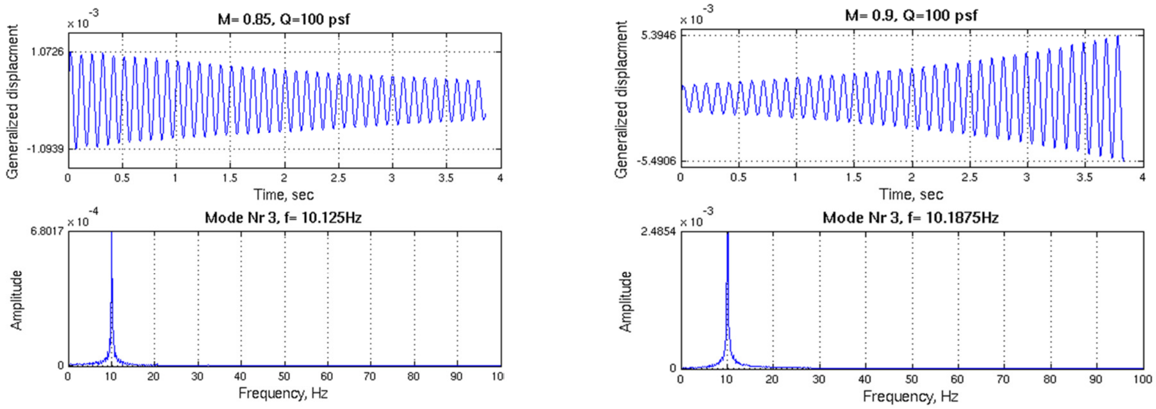

(a) M=0.85, q=100psf

(b) M=0.9, q=100psf

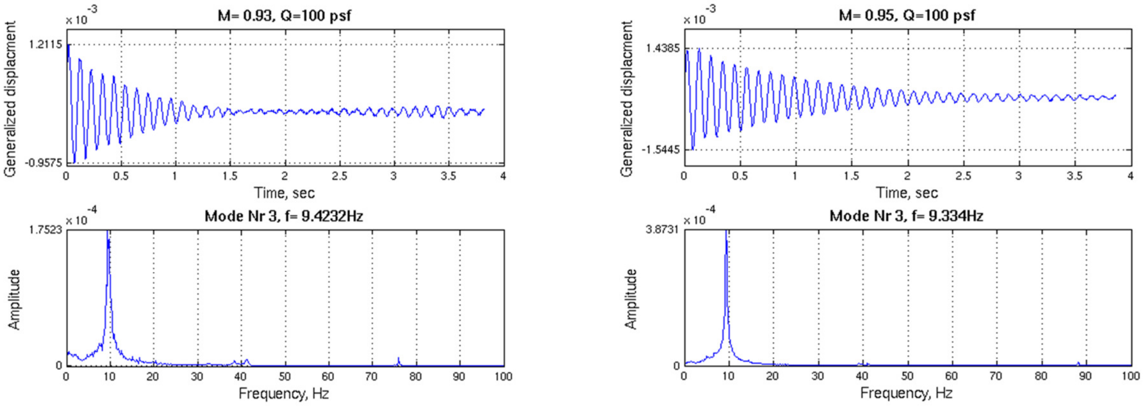

(c) M=0.93, q=100 psf

(d) M=0.95, q=100 psf

Figure 12. Analytical Results for the HS Bending Mode for various Mach Numbers, q=100 psf

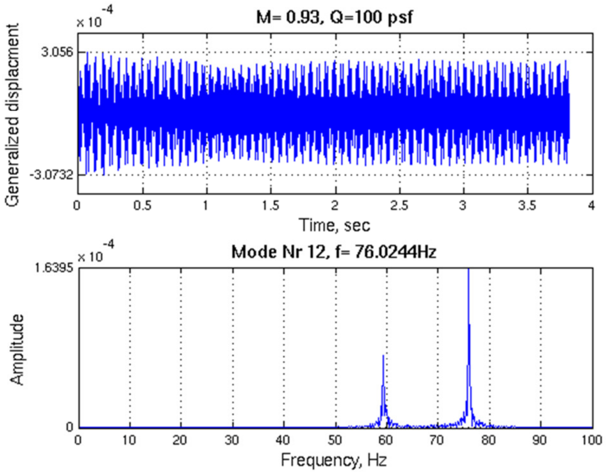

Figure 13. Analysis Results High Frequency Buffeting for M=0.93, q=76 psf

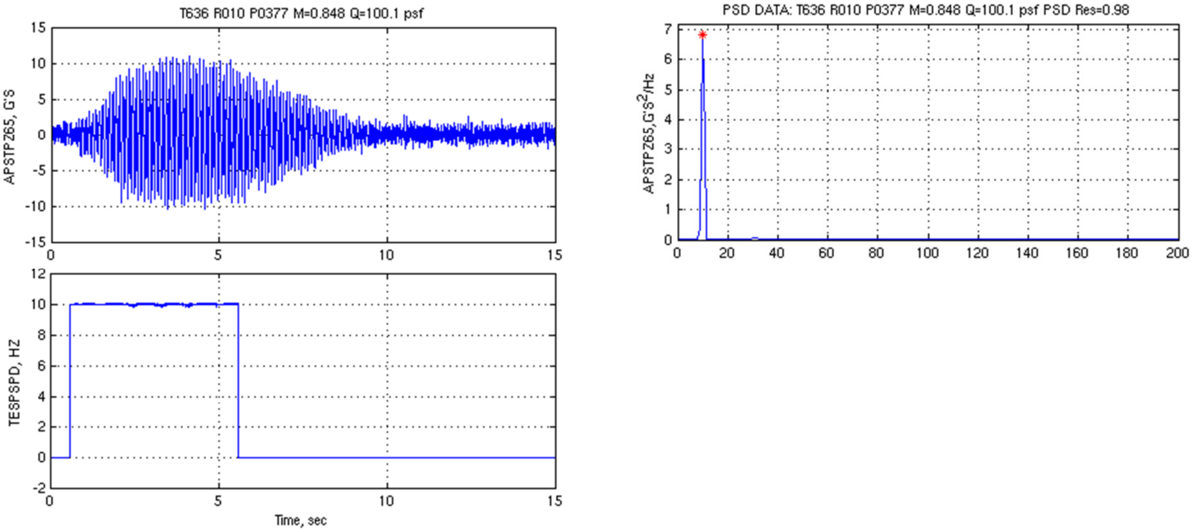

Figure 14. Test Point 377, M=0.85, q=100 psf, f=9.77 Hz

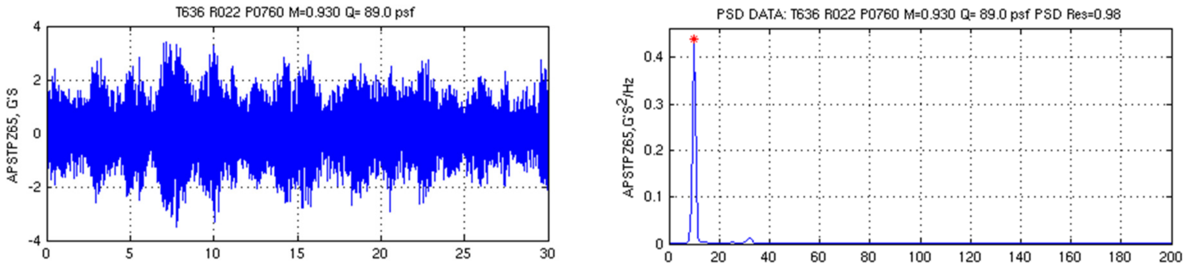

Figure 15. Test Point 760, M=0.93, q=90 psf, f=9.77 Hz

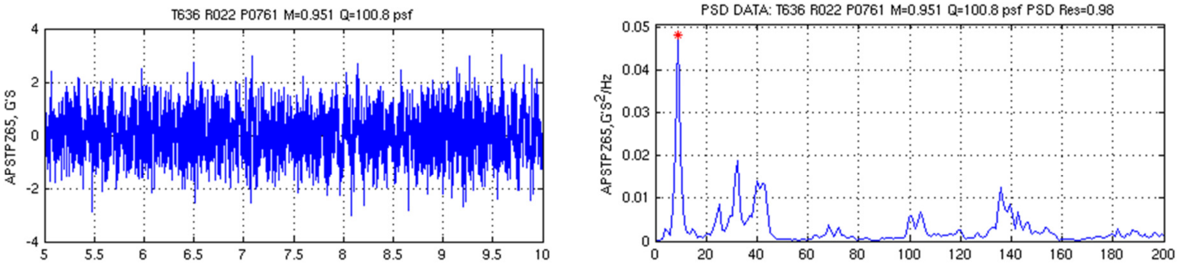

Figure 16. Test Point 761, M=0.95, q=100 psf, f=8.79 Hz

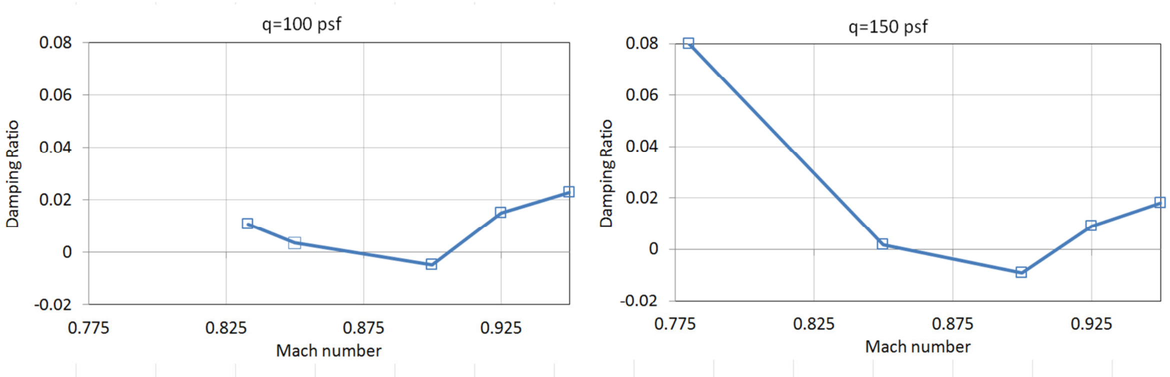

Figure 17. Analytical Damping Trend vs. Mach number

C. Mach Number Variation for q=150 psf

As in the previous section the aim was to reproduce the 10 Hz instability for M=0.9 and also to explore the instability boundaries, this time for a dynamic pressure of 150 psf.

While it was not possible to test inside the “chimney” highlighted in Figure 5, without risking damage to the model, at the end of a test day the by-pass valves were activated at M=0.96 and the 10 Hz instability regime was traversed rapidly. As illustrated in Figure 18, during test point 831, the model showed a stable behavior for M=0.96 and q=150 psf for the first 60 seconds. Shortly after activating the by-pass valves the Mach number and dynamic pressure reduced dramatically and the 10 Hz instability region was traversed quickly. On the right side of Figure 18 the time slice is expanded around the instability capturing the activation of the by-pass valves (chicken switch) and up to a few seconds after the model returned to a stable condition. One point to be mentioned about the plots concerns the data presented at the top of the plot. The data in the plot title represents an average over the complete time period. A few seconds after the by-pass valves activation, the Mach number was reduced from M=0.96 to M=0.9 and acceleration of the horizontal tail tip was amplified, the model became unstable. After further reduction of the Mach number below M=0.9 the amplitude of the tip acceleration decayed and the model returned to a stable condition. As experienced for lower dynamic pressure a lot of buffeting was present especially for high Mach Numbers.

The analysis has been performed at four Mach Numbers with the aim to reproduce the 10 Hz instability boundary for q=150psf. The time traces in Figure 19 confirm clearly the 10 Hz instability for M=0.9. The time response of the generalized displacement for M=0.85 decays with a low damping. Extracting the damping from the analysis suggests the lower boundary for the 10 Hz instability at M=0.855 and the higher boundary at M=0.92.

As experienced in the wind tunnel the instability disappears at M=0.95. The symmetric HS bending mode seems to be damped also for M=0.925, however as mentioned for q=100 psf, a high frequency buffeting is present and suggests the condition being close to the instability boundary.

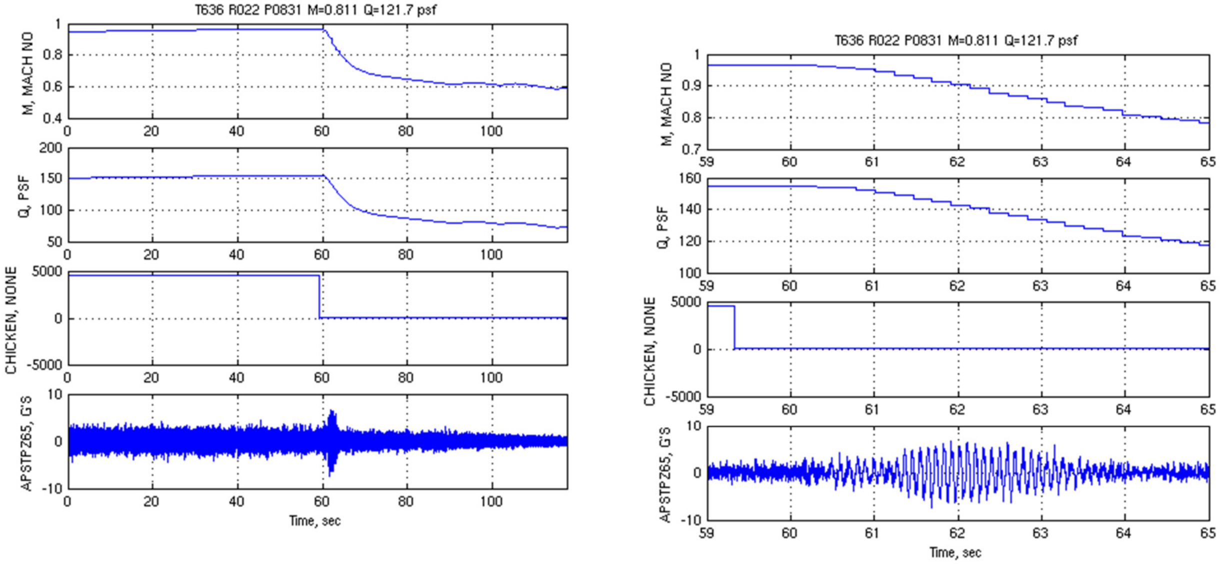

(a) Full Time Scale

(b) Expanded Time Scale

Figure 18. Test Point 831, q=150psf

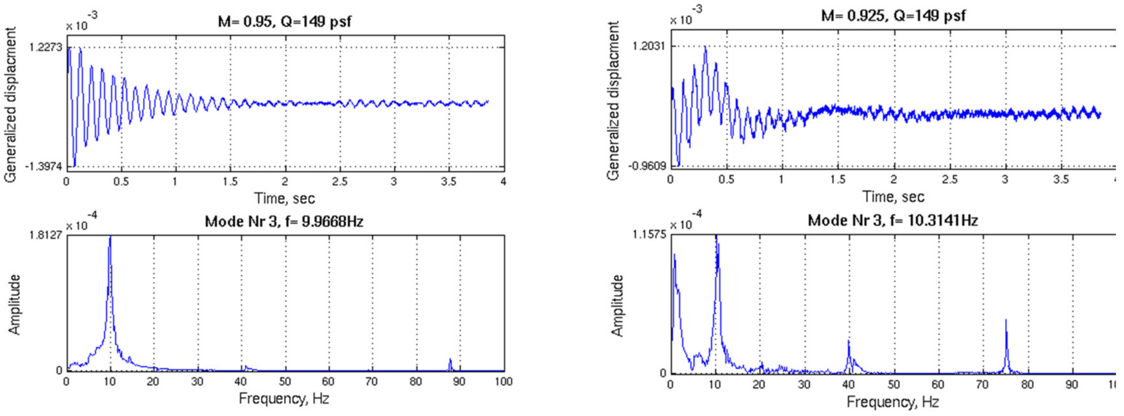

(a) M=0.95, q=150 psf

(b) M=0.925, q= 150 psf

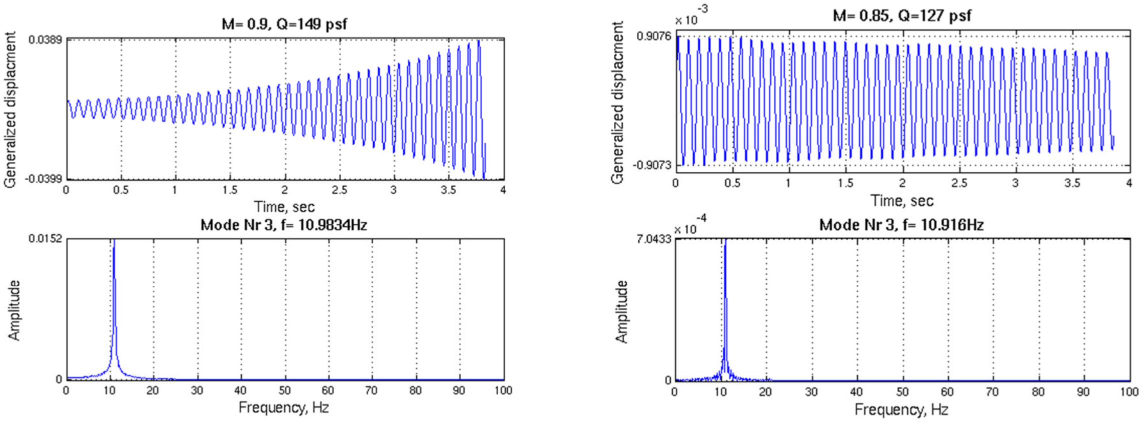

(c) M=0.9, q=150 psf

(d) M=0.85, q=120 psf

Figure 19. Analytical Results for the HS Bending Mode for various Mach Numbers, q=150 psf

D. Dynamic Pressure Variation for M=0.788

In Test point 958 a hard flutter point was encountered at q=208 psf, wherein the by-pass valves were activated. The time trace for the port elevator tip accelerometer in Figure 20 shows the increase in acceleration until the by-pass valves were activated at t=24 sec, after which the Mach Number dropped quickly and the model returned to a stable condition. The mechanism causing the instability was the horizontal stabilizer torsion coupled with the elevator rotation mode at 50 Hz. In Figure 21 the time slice is expanded around the flutter point. The PSD plots, particularly the port elevator tip accelerometer, show the 50 Hz mode quite clearly.

Figure 22 shows the damping trend from lower dynamic pressures extrapolated to the instability point. The flutter point prediction of about 208 psf from the trend line compares well to the hard flutter point tested.

The CFD analysis was performed for M=0.78 and a variation of dynamic pressures. In the middle of Figure 23 the dynamic pressure in the analysis is matched to the value in test point 958. The beating of the mode discernible in the test time traces are reproduced in the analysis. For q=150 psf the amplitude is very small and the response is damped. Increasing the dynamic pressure to 208 psf a beating of the mode suggests the condition is close to the instability boundary. By increasing the dynamic pressure further to q=250 psf the model shows an unstable condition with a dominant frequency of 52 Hz which compares well to the test result of 50 Hz.

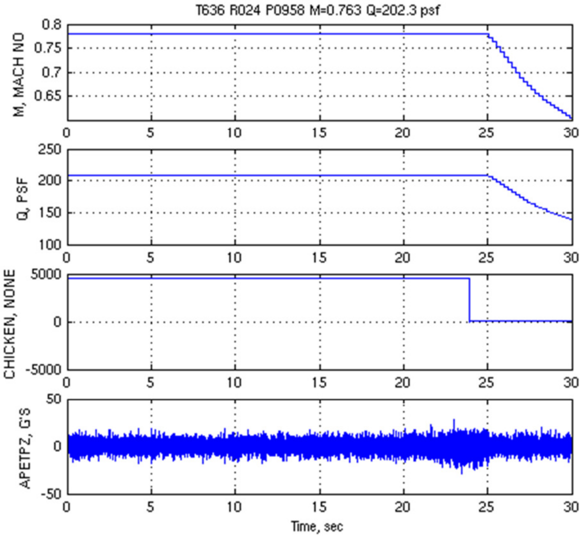

Figure 20. Test Point 958 Hard Flutter Point for M=0.78

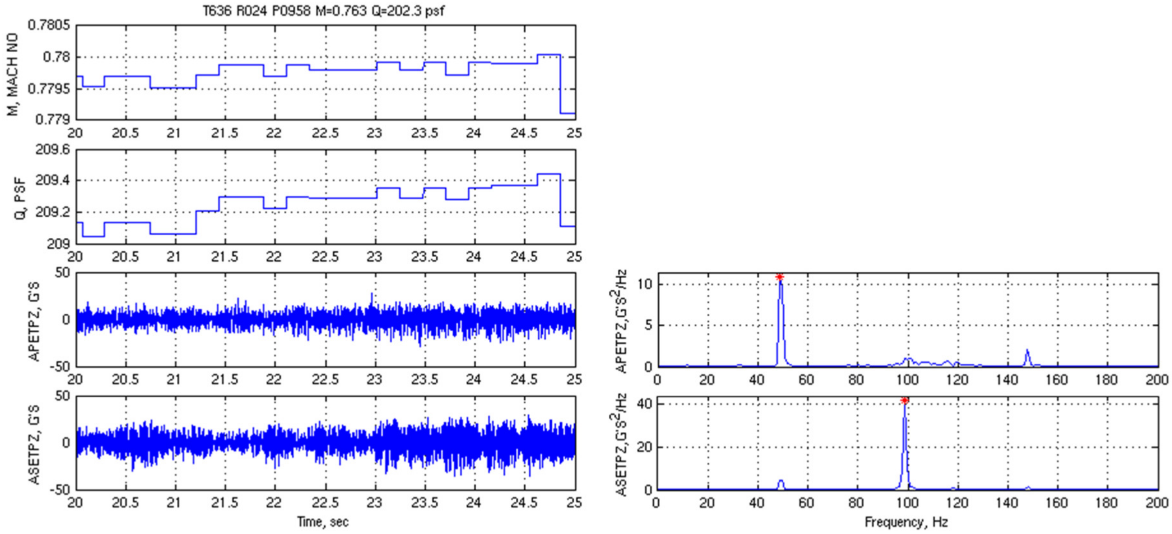

Figure 21. Test Point 958 Hard Flutter Point for M=0.78 Time Scale Extended

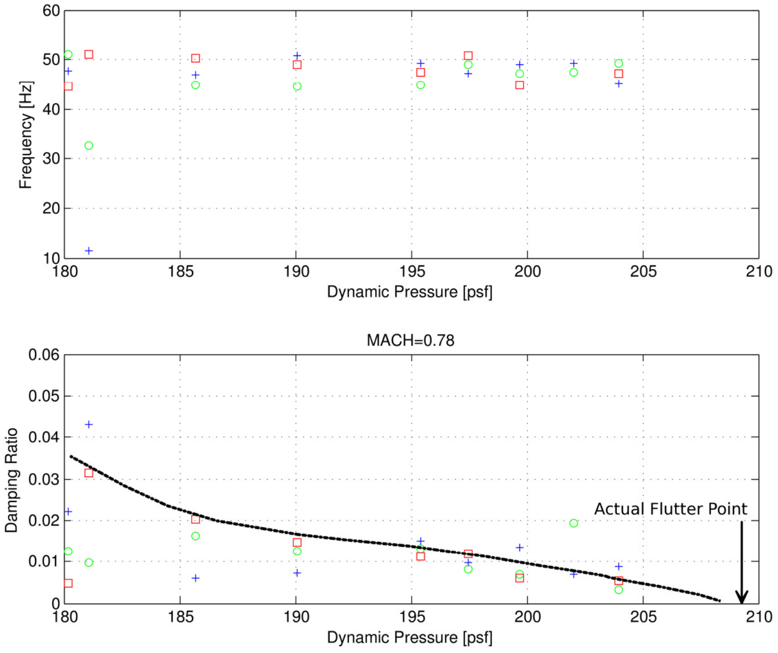

Figure 22. Damping Trend vs. Dynamic Pressure, Test Point 958

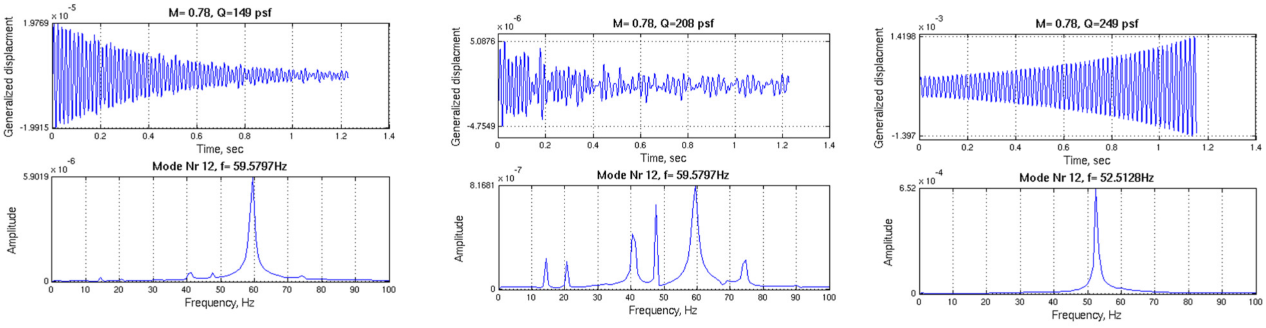

Figure 23. Analytical Results for the HS torsional mode for various q, M=0.78

E. Dynamic Pressure Variation for M=0.833

During test point 937 a second hard flutter point was encountered at q=168 psf. The time trace for the port elevator tip accelerometer in Figure 24 show the increase in acceleration, as soon as the by-pass valves were activated (t=6 sec) the Mach number dropped quickly and the model returned to a stable condition. The mechanism causing the instability was a 46 Hz coupled horizontal stabilizer torsion and elevator rotation mode, the same flutter mechanism as in the previous section. In Figure 25 the time slice is expanded around the flutter point. The dominant frequency at 46 Hz was a little bit lower than in the previous section for M=0.78.

Again the aeroelastic analysis has been performed for a variation of dynamic pressures. To understand the coupling mechanism the generalized co-ordinates for the involved modes (mode 8, 9 and 12) are plotted in Figure 26- Figure 28. For a dynamic pressure of 100 psf, well below the instability boundary, the torsional mode in Figure 28 is uncoupled and damped with a frequency of 59 Hz close to the natural frequency. In the middle of Figure 26-Figure 28 the flow parameters are matched to reflect the hard flutter point. There is a clear coupling of the HS torsional mode with the elevator rotation in Figure 28. A beating of the mode discernible in all traces matches the test data well and suggests the condition is close to the instability boundary. The dominant frequency drops from 59 Hz to 41 Hz. The last plot in Figure 28 shows the time traces for q=208 psf. The dominant frequency of 47.5 Hz and the beating of the modes match the test results extremely well.

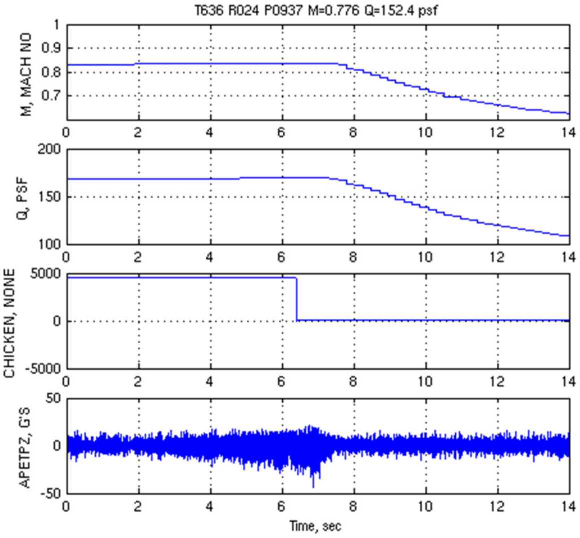

Figure 24. Test Point 937 Hard Flutter Point for M=0.833

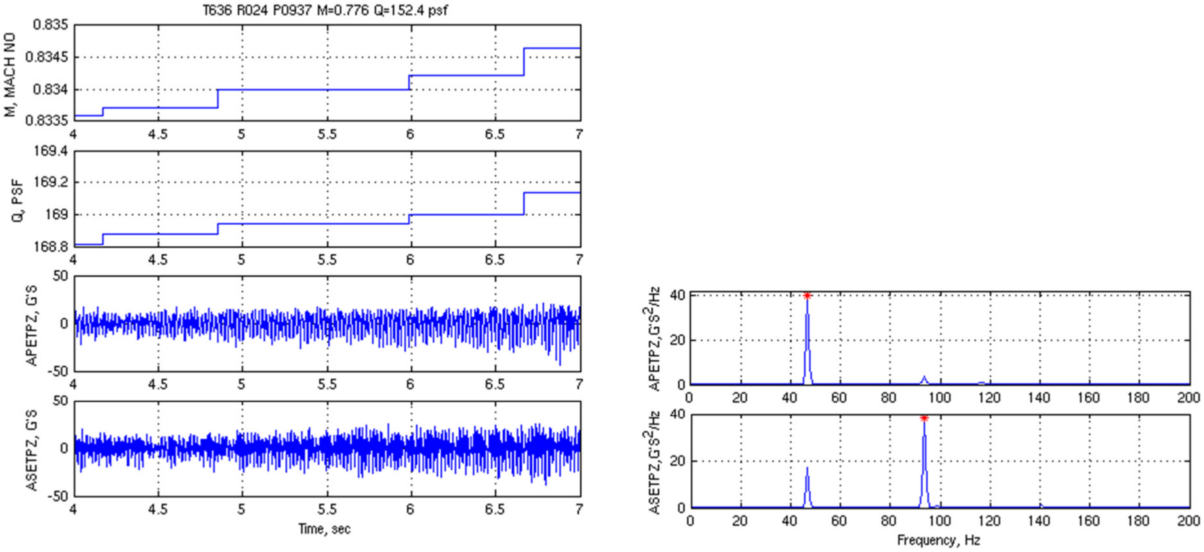

Figure 25. Test Point 937 Hard Flutter Point for M=0.833 Time Scale Extended

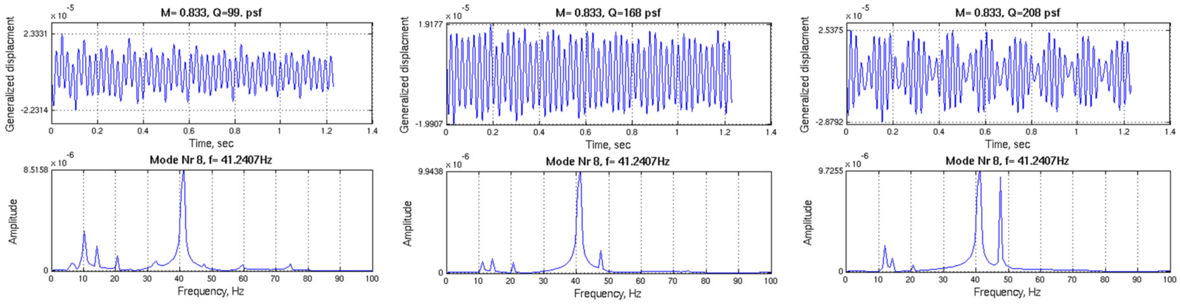

Figure 26. Analytical Results for the starboard elevator rotation mode for various q, M=0.833

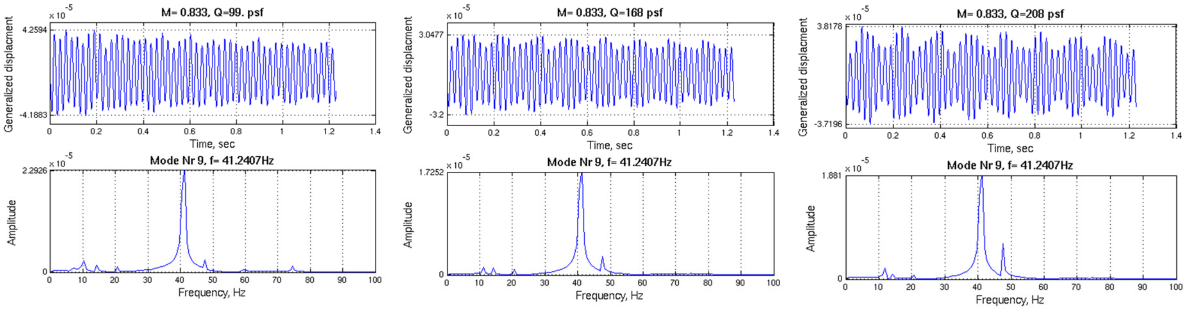

Figure 27. Analytical Results for the port elevator rotation mode for various q, M=0.833

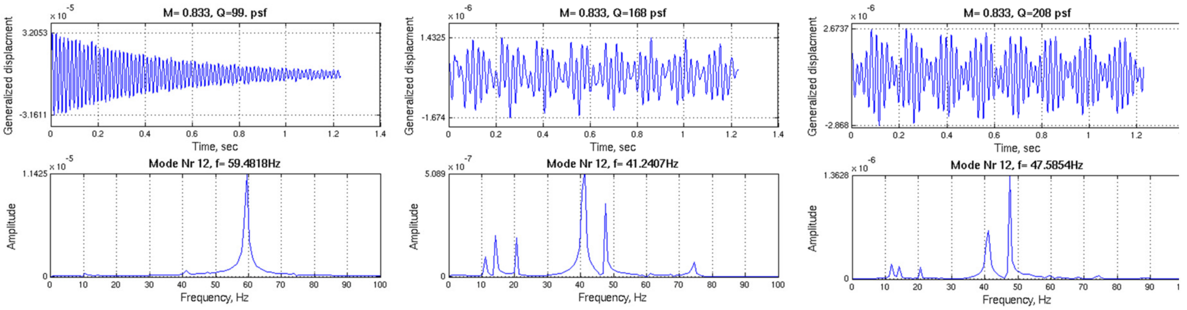

Figure 28. Analytical Results for the HS torsional mode for various q, M=0.833

V. CONCLUSION

The fluid-structure interaction path, via the aeroelastic capabilities of FUN3D, proved to be beneficial in exploring parameter spaces the testing was to not able to achieve. The CFD analysis provided an explanation to the vague boundary of the unexpected single degree of freedom instability for the first symmetric HS bending mode gained by the test. It is the author's opinion that the 10 Hz instability was caused by a shock wave emanating from the bottom fairing, impinging on the horizontal stabilizer. When the flow Mach number is between 0.85- 0.92, the shock moved to the critical location on the underside of the HS and triggers the 10 Hz mode. This is a deficiency of the design of the bottom fairing, which should have taken into account possible interaction with the model at such high transonic Mach numbers.

In addition to the single degree of freedom instability, the designed instability involving the coupling of the HS and elevator was well predicted, including sub-critical beating behavior and gives confidence that the tool is performing well and can be applied on a limited basis, to full scale flight vehicle.

ACKNOWLDEGMENT

The authors would like acknowledge the support of Gulfstream Engineering. In addition, personnel at NASA Langley, in particular Pawel Chwalowski has provided invaluable insight and assistance to the fluid-structure coupling process.

Reference

[1] *Airworthiness Standards: Transport Category Aircraft,* Code of Federal Regulations Title 14, Part 25, 2013.

[2] R. Moreno, P. Taylor and J. Newsom, "A Rigid Horizontal Tail Wind Tunnel Test for High Transonic Mach and High Frequency Unsteady Pressure Acquisition," in *53rd AIAA/ASME/ASCE/AHS/ASC Structures, Structural Dynamics and Materials Conference*, Honolulu, Hawaii, April 23-26, 2012.

[3] "http://fun3d.larc.nasa.gov," NASA Langley Research Center, November 2010. [Online].

[4] R. Bartels, C. Rumsey and R. T. Biedron, "CFL3D Version 6.4 - General Usage and Aeroelastic Analysis," NASA TM 2006-214301".

[5] W. Rodden and E. Johnson, MSC Nastran Aeroelasticity Users Guide, MSC Software Corporation, 2004.

[6] Y. Saad and M. H. Schultz, "GMRES: A Generalized Minimum Residual Algorithm for Solving Nonsymmetric Linear Systems," *SIAM Journal of Scientific and Statistical Computing, Vol. 7,* p. 856–869, 1986.

[7] P. Chwalowski, J. Florance, J. Heeg, Wieseman, C.D. and B. Perry, "Preliminary Computational Analysis of the HIRENASD Configuration in Preparation for the Aeroelastic Prediction Workshop," in *International Forum on Aeroelasticity and Structural Dynamic*, 2011.

[8] The Mathworks Inc., "Matlab Version 7.14.0 (R2012a)," Natick, Massachusetts, 2012.

[9] D. Inman, "Engineering Vibration," NJ, Prentice Hall, 2007.

[10] P. Taylor, R. Moreno, J. Newson and M.Scott, "Flutter Wing Tunnel Test At High Transonic Mach of a Flexible Empennage with Variable Control Surface Free-Play and Stiffness," in *International Forum on Aeroelasticity and Structural Dynamic*, Bristol,UK, 2013.

[11] P. R. Spalart and S. R. Allmaras, *"A One-Equation Turbulence Model for Aerodynamic Flows," La Recherche Aerospatiale, No. 1, 1994,pp 5–21.*

[12] "http://www.pointwise.com/," Pointwise, Inc.. [Online].

[13] D. Mavriplis, J. Vassberg, E. Tinoco, M. Mani, O. Brodersen, B. Eisfeld, R. Wahls, J. Morrison, T. Zickuhr, D. Levy and M. Murayama, "Grid Quality and Resolution Issues from the Drag Prediction Workshop Series," *AIAA Journal of Aircraft,* 2009.